Synthesis and evaluation of tannin-thiosemicarbazide-formaldehyde resin for selective adsorption of silver ions from aqueous solutions

Xubing Sun[1,2,3] · Shiyu Yin[1] · Yaohui You[1,2,3]

Abstract

To anchor chelating groups with nitrogen and sulfur atoms on tannin, a novel adsorbent (tannin-thiosemicarbazide-formaldehyde resin) was prepared through Mannich reaction by using blank wattle tannin, thiosemicarbazide and formaldehyde as raw materials. The adsorption behaviour of Ag^+ from aqueous solution on the resin was evaluated via batch adsorption experiments. Fourier transform infrared spectroscopy (FT–IR) and elemental analysis were applied to verify the successful immobilization. The surface morphology, thermal stability and pore structure of the resin were also characterized. The results showed that the adsorption isotherm of Ag^+ for the resin was described well by the Freundlich model. Ag^+ adsorption equilibrium was achieved within 180 min, and the kinetic data were better fitted by the pseudo-second-order kinetic equation than by the pseudo-first-order and intraparticle diffusion equations. The adsorption capacity first increased and then stabilized with increasing pH (ranging from 1.0 to 7.0), and the resin exhibited high selectivity towards Ag^+ in relation to Pb^{2+}, Cd^{2+}, Ni^{2+} and Ca^{2+}. After three regeneration and reuse cycles, the adsorption capacity reached 1.68 mmol/g (84.0% of removal efficiency). Based on the experimental results and findings from various characterization techniques, the mechanism of Ag^+ adsorption onto the resin could be attributed to inner-sphere complexation and chelation between Ag^+ and multiple electron-rich atoms (N, O, and S), in which S atoms played the most important role.

Keywords Tannin · Adsorption · Silver · Thiosemicarbazide · Mechanism

1 Introduction

Silver is a precious metal as well as a heavy metal and has been widely adopted in the electroplating, automotive, electronics, aerospace, shipbuilding, decoration, and other industries due to its excellent gloss, ductility, conductance and thermal conductivity [1, 2]. As a precious metal, silver is a nonrenewable resource, and stored silver is very rare on Earth. According to the conditions in the solar energy industry, it is expected that silver shortages will begin in 2030 with the depletion of Ag resources [3]. As a heavy metal, silver ions are very difficult to biodegrade, and can accumulate hundreds of times under the biological amplification in the food chain, posing potential risks to microorganisms, plants and humans, thereby causing damage to and impacting ecosystems [4–7].

From environmental protection, human health and sustainable resource development perspectives, there is an urgent need to effectively extract and recover Ag^+ from industrial wastewater. Numerous techniques have been employed for separating Ag^+ from wastewater, such as hydrometallurgy [8], electrochemical deposition/reduction [9–11], chemical precipitation [12], solvent extraction [13], ion exchange [14], membrane filtration [15, 16], and adsorption [17–19]. Among these techniques, adsorption is commonly applied and studied due to its the advantages of notable simplicity, adaptability and effectiveness and is regarded as the most attractive approach for removing contaminants from wastewater [20].

In recent years, chemically modified adsorbents from various agricultural byproducts used as starting materials

✉ Xubing Sun
    njtcsunxb@163.com

1   College of Chemistry and Chemical Engineering, Neijiang
    Normal University, Neijiang 641100, China

2   Sichuan Science and Technology Resources Sharing Service
    Platform of Special Agricultural Resources in Tuojiang River
    Basin, Neijiang 641100, China

3   Key Laboratory of Fruit Waste Treatment and Resource
    Recycling of the Provincial Higher Learning Institutes,
    Neijiang 641100, China

have indicated enormous potential for selective adsorption of precious metals owing to their widespread availability, cost-effectiveness, biodegradability, sustainable utilization and ecological adaptability [2, 19, 21–23]. Tannins are the most abundant source of natural aromatic compounds extracted from leaves, roots, bark, seeds and wood [24]. Due to the presence of many adjacent phenolic hydroxyl groups in their molecules, tannins are considered excellent candidates for manufacturing biosorbents for removing heavy metals and recovering precious metals [25, 26]. However, tannins are water-soluble compounds that undergo a process of immobilization/insolubility before being used as adsorbents. Insolubility of tannins can be achieved through cross-linking reactions with formaldehyde [27, 28], and their immobilization can be achieved by modifying water-insoluble matrices with tannins [29–36].

According to the hard–soft acid–base (HSAB) principle [37], the phenolic hydroxyl groups in tannin molecules are hard bases, so the affinity of tannin-based bioadsorbents for soft acids such as precious metals is expected to be low. To improve the affinity of tannin-based bioadsorbents, further chemical modifications have been implemented. Gurung et al. modified persimmon tannin gel with tetraethylenepentamine, bisthiourea and N-aminoguanidine to adsorb Au^{3+}, Pd^{2+} and Pt^{4+} [38–40]. Xiong et al. modified tannin gel with diethylamine for adsorbing precious metals from simulated wastewater [41]. Although these tannin based adsorbents containing chelating groups with N and S atoms exhibit a remarkable adsorption performance for precious metals, there are also certain drawbacks in the preparation process, such as solvent toxicity, notable time consumption, low grafting efficiency and complex synthesis processes. For example, the anchoring of tetraethylenepentamine onto persimmon tannins involves a three-step modification process. First, tannins are gelled with formaldehyde in basic media for 12 h. Then, the obtained tannin gel is subjected to an intermediate chloromethylation step in concentrated hydrochloric acid for 12 h. Finally, under sodium carbonate catalysis, the chloromethylation product reacts with tetraethylenepentamine in a heterogeneous system of dimethylformamide for 24 h [38]. Therefore, it is necessary to design and develop new approaches for anchoring chelating groups with N and S atoms onto tannins.

In this study, a tannin-thiosemicarbazide-formaldehyde resin (BTC) resin containing N and S atoms was synthesized rapidly through one-step Mannich reaction in an aqueous solution and applied for Ag^+ recovery. Characterizations were performed to validate the reaction and elucidate the characteristics of the synthesized resin. To achieve the desirable adsorption capacity for Ag^+, the influences of the pH, contact time, initial concentration of Ag^+ and ionic strength were investigated in detail by batch experiments. The adsorption kinetics and isotherms were also studied

through different models. The selectivity of BTC resin for Ag^+ adsorption was also explored in solutions containing multiple metal ions. Finally, the mechanism of Ag^+ adsorption onto the resin was determined by various characterization instruments.

2 Experimental methods

2.1 Materials and chemicals

Blank wattle tannin (BWT) was obtained from Guangxi Wuming tannin extract factory, China. Thiosemicarbazide (TC), 0.1 mol/L of $AgNO_3$ solution and 37 wt% of formaldehyde solution were purchased from Shanghai Titan Technology Co., Ltd., China. All other chemicals were of analytical grade without further purification.

2.2 Synthesis of tannin-thiosemicarbazide-formaldehyde resin

Tannin-thiosemicarbazide-formaldehyde (BTC) resin was prepared through the Mannich reaction and the proposed reaction is shown in Fig. 1. Briefly, 3 g of blank wattle tannin (BWT) was dissolved in 50 mL of pure water, followed by the addition of 2.0 g of thiosemicarbazide (TC) to the solution. After the pH was adjusted to the desired value, the temperature of the reaction was increased to 80 °C, and 2.5 mL of formaldehyde (37 wt%) was added to the flask within 30 min. The reaction was performed for 5 h. Subsequently, the sample was separated from the mixture by centrifugation and washed three times with deionized water and anhydrous ethanol. Afterwards, the obtained product was dried under vacuum at 40 °C for 24 h.

2.3 Characterization

Fourier transform infrared spectroscopy (FT–IR) of the samples was performed using an FT–IR spectrometer (FT–IR, Nicolet 6700). Thermogravimetric analysis (TGA) was performed with a TGA instrument (Netzsch, STA 449C) within the temperature range of 30–800 °C at a rate of 10 °C/min under the protection of nitrogen. The C, H, N and S contents in BWT and BTC were determined with an elemental analyser (EA, Vario Macro Cube, Elementar). The specific surface area and pore size were measured on a specific surface area tester (ASAP2020) through N_2 adsorption–desorption isotherms. The surface morphology and elemental distribution of the samples were observed by scanning electron microscopy and energy dispersive spectroscopy (SEM–EDS, FEI QUANTA 200). X-ray photoelectron spectroscopy (XPS, EscaLab 250Xi) was employed to measure the surface
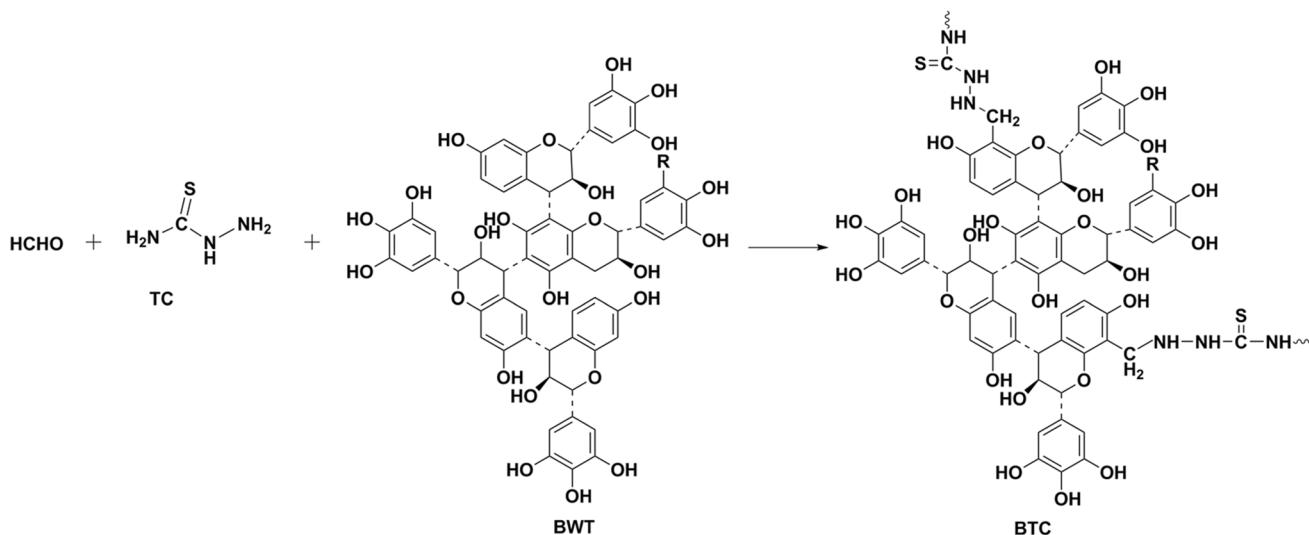
Fig.1 Synthesis route for the preparation of BTC sorbent

state and electronic structure of the BTC resin before and after Ag$^+$ adsorption, and the obtained spectra were fitted using XPSPEAK4.1 software. X-ray diffraction (XRD) patterns of the BTC resin before and after Ag$^+$ adsorption were recorded by an XRD instrument (D8-Advance). Zeta potential values were obtained with a nanoparticle size and zeta potential analyser (Litesizer 500).

2.4 Adsorption experiments

Batch adsorption experiments were performed to evaluate the adsorption behaviour of Ag$^+$ onto the BTC resin. In typical experiments, 50 mg of the BTC resin was mixed with 50 mL of silver ion solution and continuously shaken at 150 rpm and 25 °C. The effects of the pH, initial Ag$^+$ concentration, contact time, coexisting metal ions and ionic strength were investigated by varying one variable while maintaining all other parameters fixed. The influence of the pH was studied by adjusting the solution pH by either HNO$_3$ or NaOH to between 1.0 and 7.0. The mixture with a Ag$^+$ concentration of 2 mmol/L of was shaken in a thermostatic shaker for 24 h at 25 °C. Adsorption isotherm experiments were conducted with Ag$^+$ concentrations ranging from 1 to 6 mmol/L at pH 5.0 for 24 h to reach adsorption equilibrium. In the kinetics study, samples were withdrawn at periodic time intervals from the reaction mixture with 4 mmol/L Ag$^+$. The effect of coexisting metal ions was investigated by mixing 2 mmol/L Pb^{2+}, Ni^{2+}, Cd^{2+} and Ca^{2+} with 2 mmol/L Ag$^+$ at pH 2. The effect of the ionic strength was evaluated by adding solutions with different concentrations of NaNO$_3$ ranging from 0 to 0.5 mol/L, with 4 mmol/L Ag$^+$. The residual Ag$^+$ concentration after adsorption was determined by using an atomic absorption spectrophotometer (WFX 200). The adsorption

capacity (q_t) of Ag$^+$ on the BTC resin can be calculated according to Eq. (1):

$$q_t = (C_0 - C_t)V/m \tag{1}$$

where C_0 and C_t (mmol/L) are the initial concentration and concentration of the adsorbate after time t, respectively, q_t (mmol/g) is adsorption capacity after time t, m (g) is the weight of the BTC used and V (L) is the volume of the solution.

3 Results and discussion

3.1 Structure characterization

Table 1 provides the elemental analysis results for C, N, O and S in BWT and BTC. The N and S contents in BTC were 10.65% and 7.282% respectively, which far exceeded those in BWT. In addition, the C value of BTC decreased after chemical modification due to the lower C content in TC. These findings confirmed that TC was successfully attached to BWT.

Figure 2 shows the FT-IR spectra of BWT, TC and BTC. In the spectrum of BWT, the absorption band at 3412

Table 1 Elemental analysis of BWT and BTC

Sample	Element content (%)			
	C	H	N	S
BWT	49.19	4.938	0.36	0.718
BTC	44.88	4.934	10.65	7.282
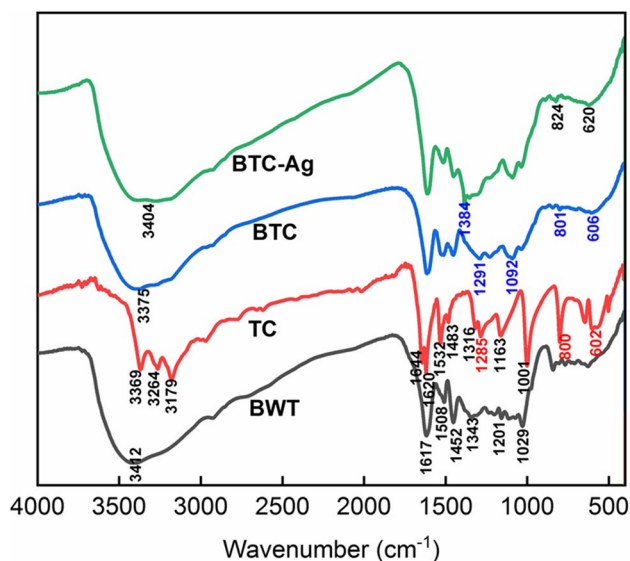
Fig.2 FT-IR spectra of BWT, TC, BTC and BTC-Ag (Ag$^+$ adsorbed by BTC)

cm^{-1} corresponded to O–H stretching vibrations, the peaks at 1617, 1508 and 1452 cm^{-1} represented characteristic adsorption bands of the benzene ring; the peaks at 1343 cm^{-1} were related to O–H bending vibrations, and the peaks at 1201 and 1029 cm^{-1} could be attributed to the C=C-O stretching vibrations and C–O–C stretching vibrations, respectively [42, 43]. Regarding TC, the absorption peaks at 3369, 3264 and 3179 cm^{-1} corresponded to N–H stretching vibrations, and those at 1644 and 1620 cm^{-1} corresponded to NH$_2$ bending vibrations. The stretching vibration bands of N–C=S(I), N–C=S(II) and N–C=S(III) were observed at 1532 and 1483 cm^{-1}, 1316, 1285 and 1163 cm^{-1}, and 1001 cm^{-1}, respectively [44, 45]. The peaks at 800 and 600 cm^{-1} could be attributed to the out-of-plane vibrations and wagging vibrations of N–H. After chemical modification, the spectral structures of BTC and BWT were similar but exhibited a slight shift in wavenumbers, which demonstrates that the core structure of BWT remained unchanged.

In addition, the spectrum of BTC contained new peaks at approximately 1291 and 1092 cm^{-1}, which were assigned to the –(C=S)–N– moiety of TC [46, 47]. The N–H out-of-plane vibration and wagging vibration peaks also appeared at 801 and 606 cm^{-1}, respectively [48]. These observations revealed that the BTC adsorbent was successfully prepared.

The thermal stabilities of BWT, TC and BTC were compared, and the results are shown in Fig. 3. BTC showed three major steps of transient weight loss at temperatures of (1) 85, (2) 210 and (3) 307 °C, corresponding to (1) moisture evaporation, (2) decomposition of the TC moiety on BTC and (3) BWT degradation, respectively [49]. Comparatively, the residue weight of BWT was greater than that of BTC. These results indicated that TC was successfully anchored on BWT.

The surface morphology of the prepared BTC adsorbent was characterized by SEM, and the results are shown in Fig. 4(a). The BTC adsorbent exhibited a spherical porous structure with a rough surface and uneven size. The pore structure and morphology are crucial parameters for an adsorbent to adsorb metal ions [50, 51], so a Brunauer–Emmett–Teller (BET) test was conducted, and the nitrogen adsorption–desorption curve is shown in Fig. 4(b). The BTC curve is a typical type IV curve, as defined by the International Union of Pure and Applied Chemistry (IUPAC) [52]. The BET surface area, total pore volume and average pore size were 67.34 m^2/g, 8.069 nm and 0.1358 cm^3/g, respectively, suggesting that the BTC resin was not a totally porous adsorbent.
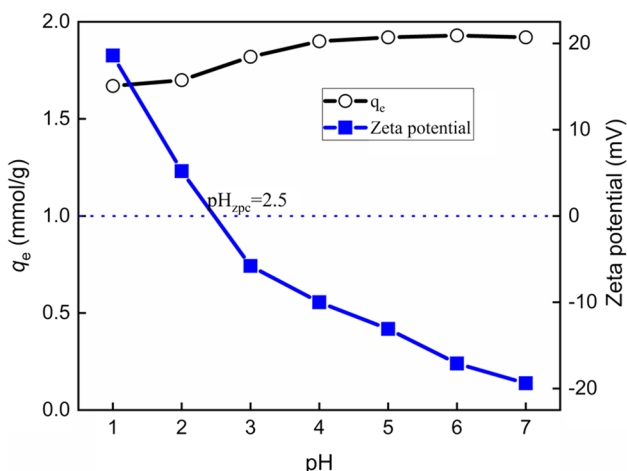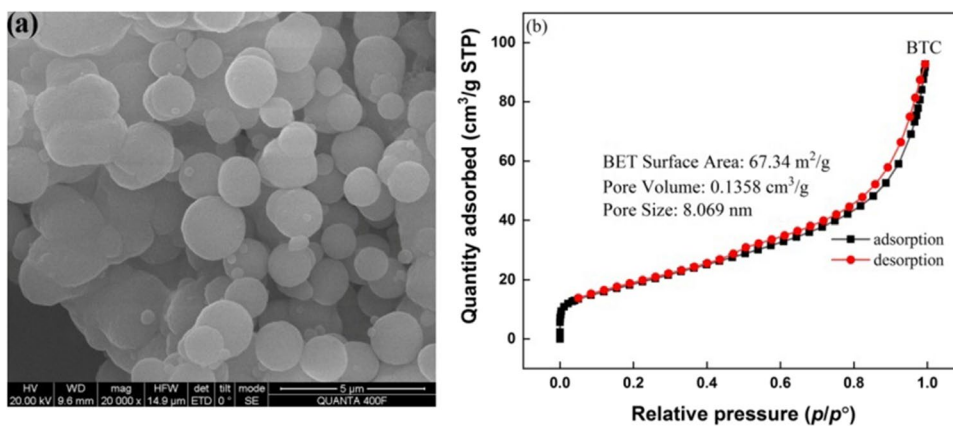
3.2 Influence of the pH on Ag$^+$ adsorption onto the BTC resin

It is widely acknowledged that the pH is a main parameter for the metal ion adsorption, because it not only affects the metal species but also influences the surface charge of the adsorbent [53]. The influences of the pH on the adsorption capacity and zeta potential of BTC were investigated at 2 mmol/L of AgNO$_3$ for 24 h. The pH was adjusted

Fig.3 (**a**) TGA and (**b**) DTG curves of BWT, TC and BTC
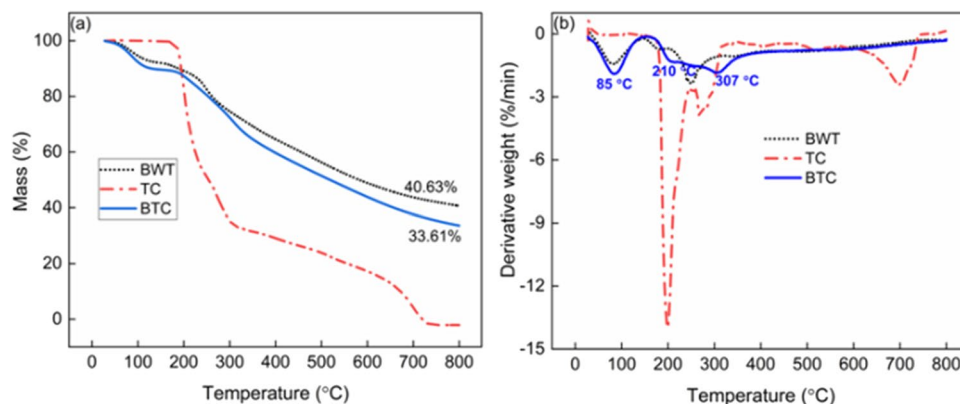
Fig.4 (a) SEM and (b) nitrogen adsorption − desorption curve of BTC

rate was greater 95% at pH 4–7. The pH_{ZPC} of BTC was measured at 2.5, indicating that the surface of BTC was positively charged at pH values less than 2.5 due to protonation of the functional groups. The positively charged BTC resin was unfavourable for the adsorption of cationic silver because of electrostatic repulsion. When the pH was increased from 3.0 to 4.0, the functional groups on the surface of BTC dissociated, and the surface was mainly negatively charged, which was promoted Ag^+ adsorption, thus increasing the adsorption capacity. However, with further increasing pH, the Ag^+ adsorption capacity changed nonsignificantly even if the zeta potential continued to decrease.

Fig.5 Influence of pH on adsorption capacity (C_0: 2 mmol/L of Ag^+; sorbent dosage: 1 g/L; T: 25 ± 1 °C; time: 24 h) and zeta potential of BTC

3.3 Influences of the contact time and adsorption kinetics

The influence of the contact time on the Ag^+ adsorption capacity is shown in Fig. 6(a). The adsorption capacity increased rapidly during the first 60 min, then slowed and reached equilibrium at 180 min. Pseudo-first-order (Eq. 2), pseudo-second-order (Eq. 3) and intraparticle diffusion models (Eq. 4) [35] were employed to fit the experimental data.

over the range of 1.0 to 7.0 to avoid the possibility of silver precipitation [54], and the results are shown in Fig. 5. The adsorption capacity for Ag^+ first increased and then stabilized with increasing pH, and the maximum removal

Fig.6 (a) Influence of contact time on adsorption capacity (C_0: 4 mmol/L of Ag^+; sorbent dosage: 1 g/L; T: 25 ± 1 °C) and fitting by Pseudo-first-order and Pseudo-second-order models; (b) fitting by Intraparticle diffusion model
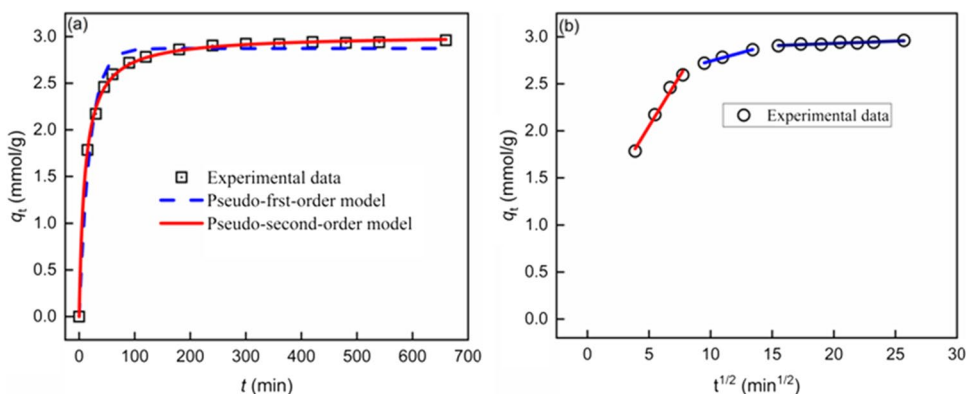
$$q_t = q_e\left(1 - e^{-k_1 t}\right) \tag{2}$$

$$q_t = \frac{q_e^2 k_2 t}{1 + q_e k_2 t} \tag{3}$$

$$q_t = k_3 \sqrt{t} + C \tag{4}$$

where q_e and q_t (mmol/g) are the amount of solute adsorbed at equilibrium and at any time t (min) per unit weight of adsorbent respectively, k_1 (min^{-1}) is the pseudo-first-order rate constant, k_2 (mmol/g min) is the pseudo-second-order rate constant and k_3 (mmol/g min$^{0.5}$) is the intraparticle diffusion rate constant.

The fitting results and calculated kinetics parameters are shown in Fig. 6(a) and Table 2, respectively. In contrast to the pseudo-first-order model, which overestimated the adsorption capacity for Ag$^+$ at the initial stage and underestimated it at the equilibrium stage, the pseudo-second order model was more suitable for describing the kinetics of Ag$^+$ adsorption onto BTC because of the greater correlation coefficient and closer equilibrium adsorption capacity between the fitting and experimental values, revealing that chemisorption was the rate-controlling step.

The adsorption kinetic data were also described by an intraparticle diffusion model, and the adsorption process was separated into three steps, as shown in Fig. 6(b). The first initial fast step corresponded to the external surface adsorption within the initial 60 min, the subsequent slow step represented intraparticle diffusion during the adsorption time ranging from 60 to 180 min, and the final equilibrium step after 240 min reflected equilibrium adsorption. Obviously, the fitting result of the first linear section deviated from the origin, indicating that Ag$^+$ adsorption on BTC was not completely governed by intraparticle diffusion [35, 55].

3.4 Influences of the initial Ag$^+$ concentration and adsorption isotherm

To evaluate the maximum adsorption capacity, the change in the adsorption capacity with different initial Ag$^+$ concentrations was investigated. As shown in Fig. 7, the amount of
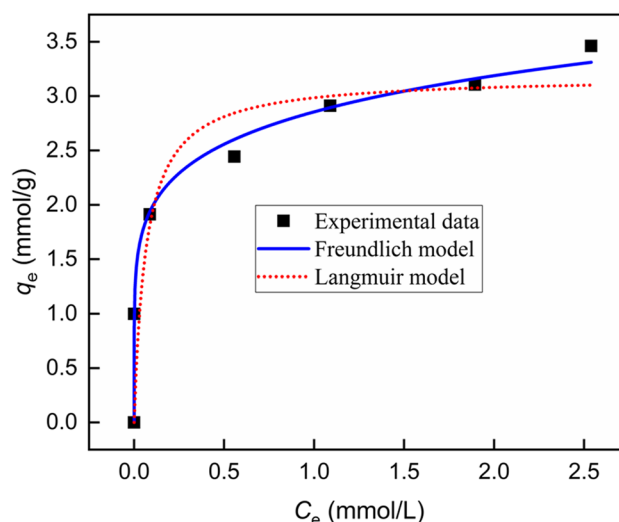
Fig.7 (a) Influence of initial Ag$^+$ concentration (C_0: 1~6 mmol/L of Ag$^+$; pH$_0$: 5.0; sorbent dosage: 1 g/L; T: 25±1 °C; time: 24 h) and fitting by Langmuir and Freundlich models

Ag$^+$ adsorbed increased with increasing initial Ag$^+$ concentration. The Langmuir (Eq. 5) and Freundlich (Eq. 6) models [35] were applied to describe the experimental data of Ag$^+$ adsorption onto the BTC resin.

$$q_e = \frac{q_{m,L} k_L C_e}{1 + k_L C_e} \tag{5}$$

$$q_e = k_F C_e^{1/n} \tag{6}$$

where q_m and q_e (mmol/g) are the maximum adsorption capacity and equilibrium amount of Ag$^+$ adsorbed per unit weight of the BTC, respectively; C_e (mmol/L) is the final equilibrium concentration of Ag$^+$; k_L (L/mmol) is the Langmuir constant; k_F (mmol/(g (L/mmol)$^{1/n}$)) and n represent the Freundlich constants.

The fitting curves and calculated parameters obtained from these two models are shown in Fig. 7 and Table 3. Notably, the Freundlich model is widely used to indicate that the adsorption occurs on heterogeneous surfaces, while the Langmuir model is based on the assumption that adsorption occurs on homogeneous monolayer surfaces with identical adsorption. As indicated in Table 3, the Freundlich model exhibited a greater correlation coefficient than the Langmuir

Table 2 Kinetics parameters for the Ag$^+$ adsorption on BTC

Kinetic models	$q_{e,cal}$	Constant		R^2
Pseudo-first-order	2.8375	$k_1 = 0.05145$		0.981
Pseudo-second-order	3.0177	$k_2 = 0.03146$		0.999
Intraparticle diffusion	—	$k_{3(1)} = 0.9815$	$C_1 = 0.2138$	0.982
		$k_{3(2)} = 2.3822$	$C_2 = 0.0360$	0.986
		$k_{3(3)} = 2.8323$	$C_3 = 0.0049$	0.848

Table 3 Parameters calculated from Freundlich and Langmuir models for Ag$^+$ adsorption on the BTC

Langmuir model			Freundlich model		
Q_{max}	k_L	R^2	k_F	n	R^2
3.1825	15.1236	0.839	2.8553	6.289	0.992

model, indicating that the BTC surface is heterogeneous and serves as another factor that favours Ag+ adsorption. In addition, the value of n was greater than 1, indicating that the adsorption process easily proceeded in aqueous medium.

To illustrate the excellent performance of BTC, the maximum adsorption capacity (Q_{max}) values in Table 4 were compared to those of other sorbents reported in the literatures. According to the Q_{max} values, BTC can be considered an effective sorbent compared with other sorbents for Ag+ removal.

The standard Gibbs energy change (ΔG^0) of Ag+ adsorption onto BTC was determined by using Eq. 7 and Eq. 8 [60].

$$k_C = \frac{k_F \rho}{1000}(\frac{10^6}{\rho})^{\left(1-\frac{1}{n}\right)} \tag{7}$$

$$\Delta G^0 = -RT\ln k_c \tag{8}$$

where k_c is the equilibrium constant; k_F (mmol/(g (L/mmol)$^{1/n}$))represents the Freundlich parameter; n is an empirical constant of Freundlich model; R is the universal gas constant (8.314 J/mol K), T is the temperature (K)and ρ is the density of pure water (1.0 g/mL).

The negative Gibbs energy change (-14.24 kJ/mol) at 298 K represents the thermodynamic feasibility and spontaneity of Ag+ adsorption onto BTC.

3.5 Influence of the ionic strength on the adsorption capacity

The effect of the ionic strength on Ag+ adsorption was investigated with NaNO$_3$ concentrations ranging from 0.005 to 0.5 mol/L. As shown in Fig. 8(a), the adsorption capacity for Ag+ gradually increased with increasing NaNO$_3$ concentration. Generally, if an outer-sphere surface complex is formed between the adsorbent and adsorbate by ion exchange or electrostatic forces, the adsorption capacity decreases with increasing ionic strength, while for inner-sphere surface complexes, the adsorption capacity increases with increasing ionic strength or is independent of the ionic strength [61, 62]. Therefore, the observed positive influence of the ionic strength suggested that Ag+ adsorption onto BTC entailed an inner-sphere adsorption mechanism through a coordinate-covalent bond between the ligand and Ag+, which is consistent with earlier research of Dong et al. [53].

Table 4 Comparison of the adsorption capacity with the various sorbent

Sorbent	Q_{max}(mmol/g)	Equilibrium time (min)	Ref
Melamine- formaldehyde- thiourea resin	0.951	65	[18]
Multi-thiolated cage mesoporous monoliths	1.67	20	[56]
Superparamagnetic carbon	0.57	60	[57]
2-Mercaptobenzimidazole magnetic chitosan	2.02	1920	[23]
polymer functionalized by 3-amino-1,2,4-triazole-5-thiol and glutaraldehyde	4.16	400	[58]
Ag+ imprinted chitosan gel beads	0.83	2880	[59]
BTC	3.18	180	This work

Fig.8 (a) Effect of ionic strength on Ag+ adsorption onto BTC (C_0: 2 mmol/L of Ag+; pH$_0$: 2.0; sorbent dosage: 1 g/L; T: 25 ± 1 °C; time: 24 h); (b) Selective adsorption of BTC for Ag+ (C_0: 4 mmol/L of Ag+; sorbent dosage: 1 g/L; T: 25 ± °C; time: 24 h)
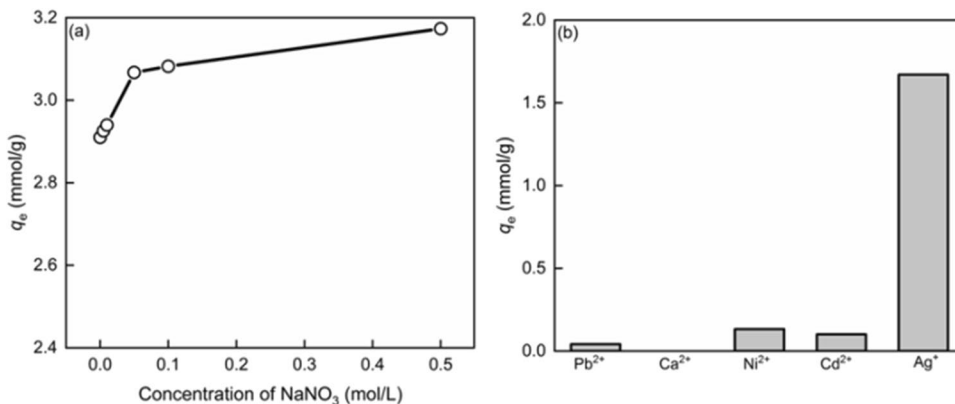
3.6 Adsorption selectivity

Considering the complexity of the real aquatic environment, the selectivity of the BTC resin for Ag^+ adsorption was evaluated in a mixed solution containing Ag^+, Pb^{2+}, Ca^{2+}, Ni^{2+}, and Cd^{2+} at the same ratios. Figure 8(b) shows that the Ag^+ removal rate of the BTC resin exceeded 95%, while the removal rates for the other metal ions were less than 10%, revealing that BTC exhibited high selectivity for the Ag^+ adsorption from the mixed solution.

3.7 Regeneration and reuse study of the BTC

To regenerate and reuse BTC, a desorption experiment was conducted by immerging BTC-Ag in a 0.5 mol/L thiourea–0.1 mol/L HNO_3 mixed solution for 1 h and washing with ultrapure water for five times [45, 48]. The regenerated BTC was reused during the next cycle. After three regeneration and reuse cycles, the adsorption capacities were 1.91, 1.82 and 1.68 mmol/g, corresponding to removal efficiencies of 95.5%, 91.1% and 84.1%, respectively. Therefore, the BTC adsorbent possessed favourable stability and reusability for Ag^+ recovery from wastewater.

3.8 Adsorption mechanism

The variations in the surface morphology and element distribution on the BTC resin after Ag^+ uptake were characterized by SEM–EDS. As shown in Fig. 9(a), the spherical morphology of BTC remained unchanged after Ag^+ adsorption.

The elements on BTC after Ag^+ uptake were examined by EDS (Fig. 9(b)), and the EDS spectrum revealed that the main constituents were C, O, N, S and Ag, demonstrating successful Ag^+ adsorption onto the BTC surface. The corresponding atomic percentages were 56.47%, 18.11%, 9.06%, 7.54% and 8.82%, respectively. The atomic percentage ratio of S to Ag was less than 1, indicating that other functional groups participate in Ag^+ adsorption.

The distributions of the C, O, N, S and Ag on the BTC-Ag surface were also explored and are shown in Fig. 9 (c-g). Elemental Ag exhibited consistency with S, providing evidence that S atoms on the BTC played an important role in Ag^+ adsorption. According to the soft-hard acid–base (SHAB) theory, Ag^+ (a soft metal ion) exhibits a greater affinity for hard bases with donor atoms in the order of $O < N < S$ [37, 46, 63, 64].

To examine the adsorption mechanism, the TF-IR spectrum of BTC after Ag^+ adsorption (BTC-Ag) was obtained. As shown in Fig. 2, compared to the spectrum of the BTC, a new peak at 1384 cm^{-1} related to Ag–S stretching vibration was observed in the spectrum of BTC-Ag [65]. In addition, the peak attributed to phenolic hydroxyl groups became narrower and shifted from 3375 to 3404 cm^{-1}. The peaks attributed to N–H out-of-plane vibrations and wagging vibrations shifted from 801 and 606 cm^{-1} to 824 and 620 cm^{-1}, respectively. These observations indicated that O, S and N atoms on the BTC surface participated in Ag^+ adsorption.

XRD analysis of the BTC resin before and after Ag^+ adsorption was performed, and the results are shown in Fig. 10(a). BTC exhibited an amorphous structure with a

Fig.9 (a) SEM, (b) EDS and (c-g) elements distribution of BTC after Ag^+ adsorption
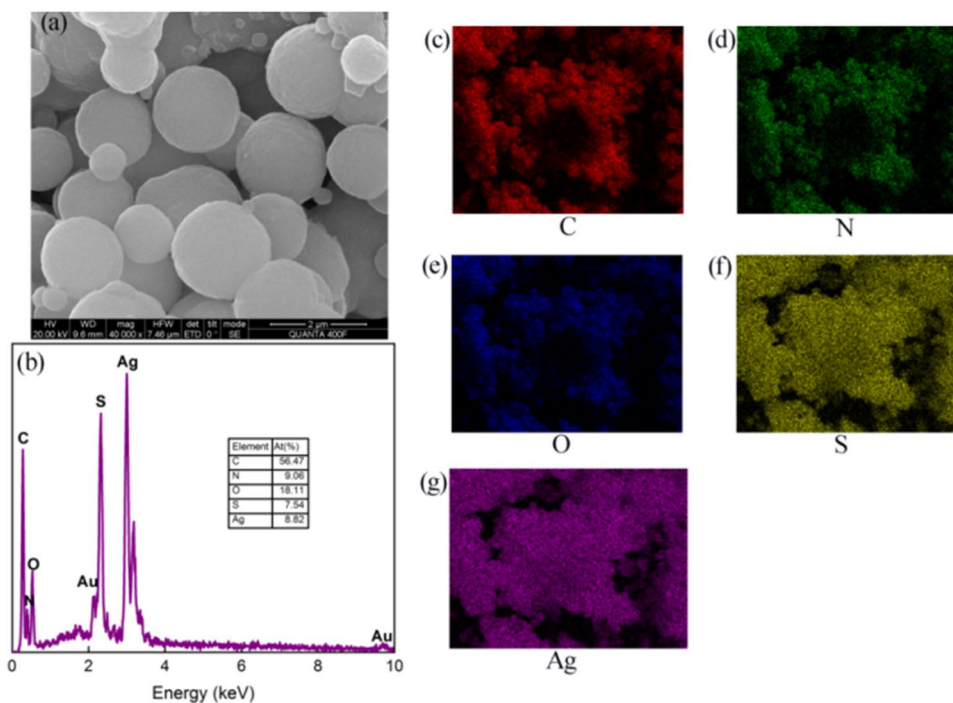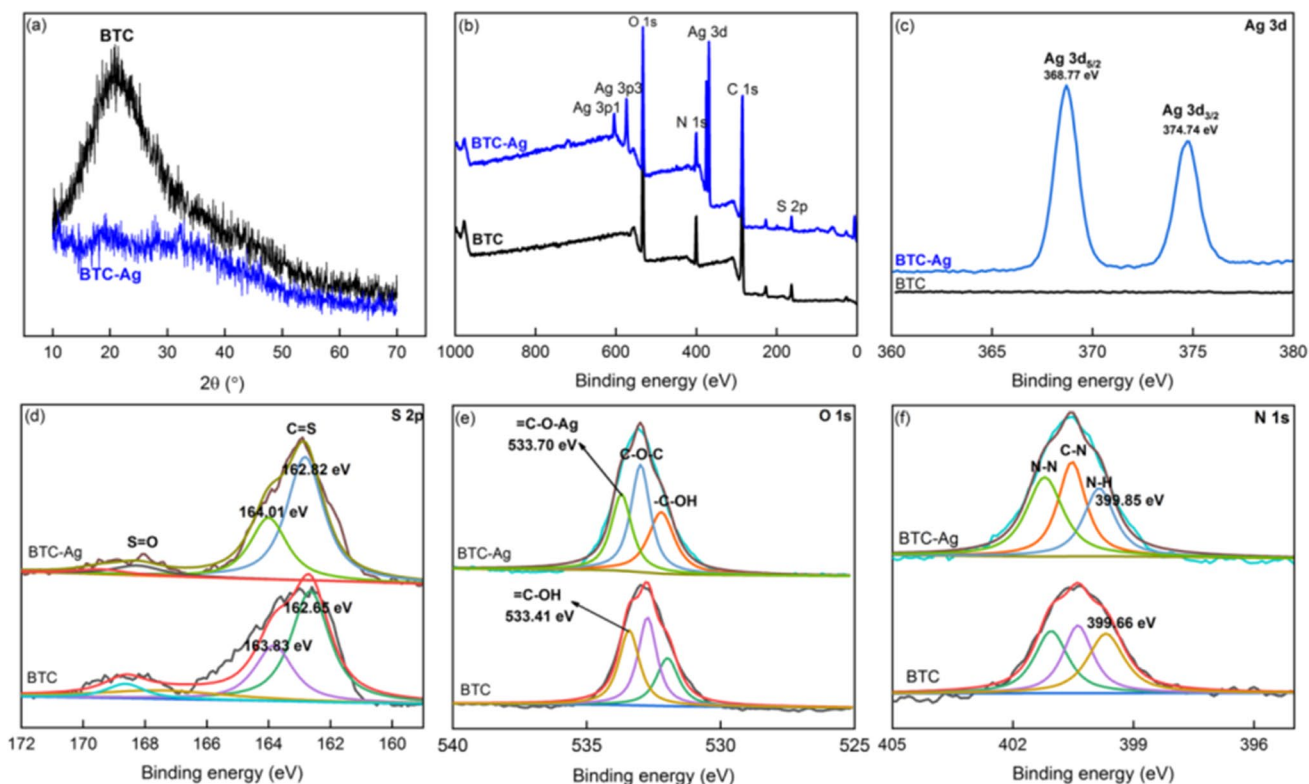
Fig. 10 (a) XRD patterns of BTC and BTC-Ag (Ag⁺ adsorbed by BTC);(b) XPS survey spectra of BTC and BTC-Ag; (c) higher resolution of Ag 3d, S 2p, O 1s and N 1s spectra of BTC and BTC-Ag

**Table 5** Relative atomic ratios of BTC and BTC-Ag measured by XPS

Samples	C(%)	O(%)	N(%)	S(%)	Ag(%)
BTC	63.02	22.91	10.73	3.36	0
BTC-Ag	58.47	22.44	11.19	3.46	4.43

broad hollow peak at $2\theta = 22°$, which indicates the presence of polar functional groups [66]. After Ag⁺ adsorption, no new peak was observed, and the intensity of the peak at $2\theta = 22°$ substantially decreased. This could be ascribed to the formation of complexes between the phenolic groups on the BTC surface and silver ions, which reduces the polarity of the functional group [66].

To better assess the mechanism by which Ag⁺ could chelate with the functional groups on BTC, XPS measurements of BTC before and after Ag⁺ adsorption were performed. Figure 10(b) and Table 5 provide the XPS survey spectra and corresponding atomic ratios of the raw BTC and BTC-Ag measured by XPS. Before Ag⁺ adsorption, four peaks at 284.8, 533.07, 400.58 and 162.93 eV corresponded to C 1 s, O 1 s, N 1 s and S 2p, respectively, were observed in the spectrum of fresh BTC, further illustrating the successful introduction of TC into BWT. After

Ag⁺ adsorption, a new peak at a binding energy of 368.7 eV related to the representative peak of Ag 3d appeared. The notable signals in the deconvolution of Ag 3d orbital (Fig. 10(c)) provided evidence of Ag⁺ adsorption onto the BTC (Table 5), which is consistent with the SEM–EDS results. In addition, the shift in the electron binding energy in the high-resolution XPS spectra indicated a change in bonding around an atom. Figure 10(d), (e) and (f) show the S 2p, O 1s and N 1s XPS spectra, respectively, of BTC and BTC-Ag. The S 2p XPS spectra were deconvoluted into two distinct different component peaks, which could be attributed to S = O and C = S. The binding energies of C = S at 162.82 and 164.01 eV in pristine BTC shifted to 162.65 and 163.83 eV, respectively, after Ag⁺ adsorption, suggesting a possible chemical change of in S once Ag⁺ was adsorbed onto BTC [50]. Similar phenomena were further confirmed by shifts in the binding energies of O 1 s and N 1 s before and after Ag⁺ adsorption, revealing that N, O and S participated in Ag⁺ adsorption, which is well consistent with the FT-IR results.

As described in this section, the mechanism of Ag⁺ adsorption onto the as-prepared BTC resin, as shown in Fig. 11 could be attributed to the chelation between Ag⁺ and multiple electron-rich atoms (N, O, and S), in which the S atom played the most important role.
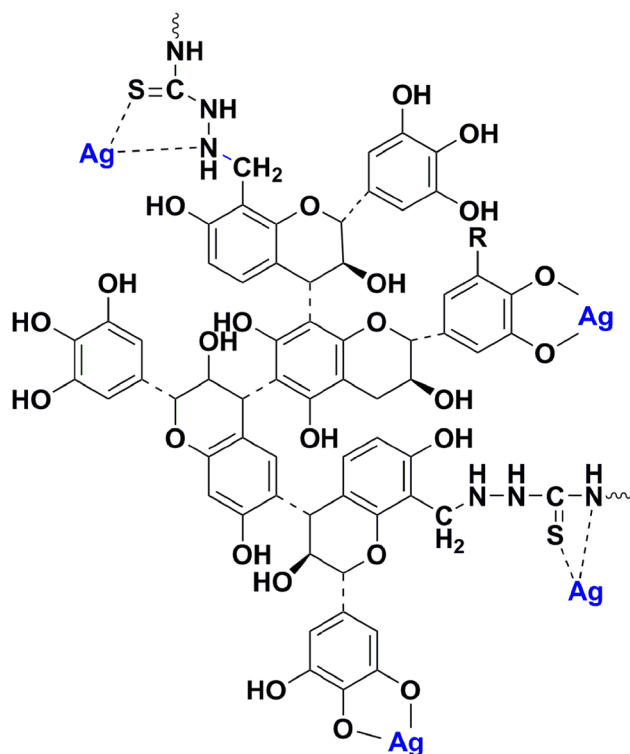
Fig.11 Suggested mechanism of Ag$^+$ adsorption onto BTC

4 Conclusions

A tannin-based adsorbent (BTC) with nitrogen and sulfur atoms was successfully fabricated through the Mannich reaction. The BTC adsorbent exhibited high adsorption capacity and selectivity for Ag$^+$ from solutions in the presence of other metals, such as Pb^{2+}, Ni^{2+}, Ca^{2+} and Cd^{2+}. The adsorption isotherm of Ag$^+$ for BTC was described well by the Freundlich model, and the kinetic data of Ag$^+$ adsorption onto the resin were suitably fitted by the pseudo-second-order model. Furthermore, batch experiments and various characterizations revealed that the interaction mechanism between the BTC resin and Ag$^+$ involved inner-sphere complexation and chelation between Ag$^+$ and multiple electron-rich atoms (N, O, and S). Among the multiple electron-rich atoms, the S atom played the most important role. In conclusion, this work described a one-step method in an aqueous solution for developing a tannin based absorbent containing nitrogen and sulfur atoms for silver recovery.

Authors' contributions X.B. Sun developed the concept, designed the experiments and drafted the manuscript. S.Y. Yin performed the experiments and acquired the data. Y.H. You reviewed the manuscript.

Declarations

Competing interests The authors declare no competing interests.

Conflict of interest The authors declare that they have no known competing financial interests or personal relationships that could have appeared to influence the work reported in this paper.

Ethical approval Not applicable.

References

1. Nakhjiri, A.T., et al.: Recovery of precious metals from industrial wastewater towards resource recovery and environmental sustainability: A critical review. Desalination **527**, 115510 (2022)
2. Biswas, F.B., et al.: Selective recovery of silver and palladium from acidic waste solutions using dithiocarbamate-functionalized cellulose. Chem. Eng. J. **407**, 127225 (2021)
3. Pilśniak-Rabiega, M., Wolska, J.: Silver(I) recovery on thiomorpholine - modified functional polymer. Physicochem. Probl. Miner. Process. **58**, 156609 (2022)
4. Vasileiadis, S., et al.: Silver toxicity thresholds for multiple soil microbial biomarkers. Environ. Sci. Technol. **52**, 8745–8755 (2018)
5. Eckelman, M.J., Graedel, T.E.: Silver emissions and their environmental impacts: a multilevel assessment. Environ. Sci. Technol. **41**, 6283–6289 (2007)
6. Tortella, G.R., et al.: Silver nanoparticles: toxicity in model organisms as an overview of its hazard for human health and the environment. J. Hazard. Mater. **390**, 121974 (2020)
7. Kalčíková, G., et al.: An environmental concentration of aged microplastics with adsorbed silver significantly affects aquatic organisms. Water Res. **175**, 115644 (2020)
8. Birloaga, I., Vegliò, F.: Overview on hydrometallurgical procedures for silver recovery from various wastes. J. Environ. Chem. Eng. **6**, 2932–2938 (2018)
9. Zimmermann, P., et al.: Selective recovery of silver ions from copper-contaminated effluents using electrodialysis. Desalination **572**, 117108 (2024)
10. Mitov, M., et al.: Silver recovery by microbial electrochemical snorkel and microbial fuel cell. Electrochim. Acta **408**, 139941 (2022)
11. Wang, Z., et al.: Recovery of silver from dilute effluents via electrodeposition and redox replacement. J. Electrochem. Soc. **166**, 266–274 (2019)
12. John, M., et al.: Recovery of Ag and Au from synthetic and industrial wastewater by 2-step ferritization and Lt-delafossite process via precipitation. J. Water Process. Eng. **30**, 100532 (2019)
13. Cho, S.Y., Kim, T.Y., Sun, P.P.: Recovery of silver from leachate of silicon solar cells by solvent extraction with TOPO. Sep. Purif. Technol. **215**, 516–520 (2019)
14. Virolainen, S., et al.: Ion exchange recovery of silver from concentrated base metal-chloride solutions. Hydrometallurgy **152**, 100–106 (2015)
15. Yi, M., et al.: In-situ silver recovery for biofouling mitigation with catechol-assisted nanofiltration membrane. Desalination **547**, 116233 (2023)
16. Huang, X., et al.: Fabrication of polyvinylidene fluoride and acylthiourea composite membrane and its adsorption performance and mechanism on silver ions. Sep. Purif. Technol. **315**, 123675 (2023)

17. Shao, P., et al.: Mixed-valence molybdenum oxide as a recyclable sorbent for silver removal and recovery from wastewater. Nat. Commun. **14**, 1365 (2023)

18. Abd El-Ghaffar, M.A., et al.: Extraction and separation studies of silver(I) and copper(II) from their aqueous solution using chemically modified melamine resins. Hydrometallurgy **96**, 27–34 (2009)

19. Huang, Y., et al.: Anion-synergistic adsorption enhances the selective removal of silver ions from complex wastewater by chitosan-coated magnetic silica core-shell nanoparticles. J. Clean. Prod. **339**, 130777 (2022)

20. Wang, P., et al.: Magnetic mesoporous calcium carbonate-based nanocomposites for the removal of toxic Pb(II) and Cd(II) ions from water. ACS Appl. Nano Mater. **3**, 1272–1281 (2020)

21. Fan, J., et al.: Selective adsorption and recovery of silver from acidic solution using biomass-derived sulfur-doped porous carbon. ACS Appl. Mater. Interfaces **15**, 40088–40099 (2023)

22. Ghomi, G.A., et al.: Biosorpion for sustainable recovery of precious metals from wastewater. J. Environ. Chem. Eng. **8**, 103996 (2020)

23. Elwakeel, K.Z., et al.: 2-Mercaptobenzimidazole derivative of chitosan for silver sorption – Contribution of magnetite incorporation and sonication effects on enhanced metal recovery. Chem. Eng. J. **403**, 126265 (2021)

24. Arbenz, A., Averous, L.: Chemical modification of tannins to elaborate aromatic biobased macromolecular architectures. Green Chem. **17**, 2626–2646 (2015)

25. Kavitha, V.U., Kandasubramanian, B.: Tannins for wastewater treatment. SN Appl. Sci. **2**, 1081 (2020)

26. Bacelo, H.A.M., Santos, S.C.R., Botelho, C.M.S.: Tannin-based biosorbents for environmental applications – A review. Chem. Eng. J. **303**, 575–587 (2016)

27. Kim, Y.H., Nakano, Y.: Adsorption mechanism of palladium by redox within condensed-tannin gel. Water Res. **39**, 1324–1330 (2005)

28. Ogata, T., Nakano, Y.: Mechanisms of gold recoveryfrom aqueous solutions using a novel tannin gel adsorbent synthesized from natural condensed tannin. Water Res. **39**, 4281–4286 (2005)

29. Sun, X., et al.: Adsorptive removal of Cu(II) from aqueous solutions using collagen-tannin resin. J. Hazard. Mater. **186**, 1058–1063 (2011)

30. Huang, X., Liao, X.P., Shi, B.: Hg(II) removal from aqueous solution by bayberry tannin-immobilized collagen fiber. J. Hazard. Mater. **170**, 1141–1148 (2009)

31. Huang, X., et al.: Adsorptive recovery of Au^{3+} from aqueous solutions using bayberry tannin-immobilized mesoporous silica. J. Hazard. Mater. **183**, 793–798 (2010)

32. Wang, Y., et al.: Enhanced adsorption of Pb(II) ions from aqueous solution by persimmon tannin-activated carbon composites. J. Wuhan Univ. Technol. Mater. Sci. Ed. **28**, 650–657 (2013)

33. Xu, Q., et al.: Adsorption of Cu (II), Pb (II) and Cr (VI) from aqueous solutions using black wattle tannin-immobilized nanocellulose. J. Hazard. Mater. **339**, 91–99 (2017)

34. Fan, R., Min, H., Hong, X.: Plant tannin immobilized $Fe_3O_4@SiO_2$ microspheres: a novel and green magnetic bio-sorbent with superior adsorption capacities for gold (III) and palladium(II). J. Hazard. Mater. **364**, 780–790 (2019)

35. Liu, F., et al.: Au(III) adsorption and reduction to gold particles on cost-effective tannin acid immobilized dialdehyde corn starch. Chem. Eng. J. **370**, 228–236 (2019)

36. Wang, Z., et al.: Equilibrium, kinetics and mechanism of Au^{3+}, Pd^{2+} and Ag^+ ions adsorption from aqueous solutions by graphene oxide functionalized persimmon tannin. Mat. Sci. Eng. C-Mater. **79**, 227–236 (2017)

37. Pearson, R.G.: Hard and soft acids and bases. J. Am. Chem. Soc. **85**, 3533–3539 (1963)

38. Gurung, M., et al.: Persimmon tannin-based new sorption material for resource recycling and recovery of precious metals. Chem. Eng. J. **228**, 405–414 (2013)

39. Gurung, M., et al.: Selective recovery of precious metals from acidic leach liquor of circuit boards of spent mobile phones using chemically modified persimmon tannin gel. Ind. Eng. Chem. Res. **51**, 11901–11913 (2012)

40. Gurung, M., et al.: N-aminoguanidine modified persimmon tannin: a new sustainable material for selective adsorption, preconcentration and recovery of precious metals from acidic chloride solution. Bioresour. Technol. **129**, 108–117 (2013)

41. Xiong, Y.C., et al.: Selective recovery of precious metals by persimmon waste chemically modified with dimethylamine. Bioresour. Technol. **100**, 4083–4089 (2009)

42. Li, X., et al.: Chitosan modification persimmon tannin bioadsorbent for highly efficiency removal of Pb(II) from aqueous environment: the adsorption equilibrium, kinetics and thermodynamics. Environ. Technol. **40**, 112–124 (2019)

43. Ricci, A., et al.: Application of fourier transform infrared (FTIR) spectroscopy in the characterization of tannins. Appl. Spectrosc. Rev. **50**, 407–442 (2015)

44. Wang, F., et al.: Superior Au-adsorption performance of aminothiourea-modified waste cellulosic biomass. J. Cent. South Univ. **25**, 2992–3003 (2018)

45. Liu, P., et al.: Adsorption of silver ion from the aqueous solution using a polyvinylidene fluoride functional membrane bearing thiourea groups. J. Water Process Eng. **34**, 101184 (2020)

46. Lin, G., et al.: Synthesis and evaluation of thiosemicarbazide functionalized corn bract for selective and efficient adsorption of Au(III) from aqueous solutions. J. Mol. Liq. **258**, 235–243 (2018)

47. Zhou, L., Liu, J., Liu, Z.: Adsorption of platinum(IV) and palladium(II) from aqueous solution by thiourea-modified chitosan microspheres. J. Hazard. Mater. **172**, 439–446 (2009)

48. Xiong, Y., et al.: Selective recovery of Ag(I) coordination anion from simulate nickel electrolyte using corn stalk based adsorbent modified by ammonia–thiosemicarbazide. J. Hazard. Mater. **301**, 277–285 (2016)

49. Deng, S., et al.: Polyacrylonitrile-based fiber modified with thiosemicarbazide by microwave irradiation and its adsorption behavior for Cd(II) and Pb(II). J. Hazard. Mater. **307**, 64–72 (2016)

50. Chen, Z., et al.: Synthesis of silica supported thiosemicarbazide for Cu(II) and Zn(II) adsorption from ethanol: A comparison with aqueous solution. Fuel **286**, 119287 (2021)

51. Wang, Z.H., et al.: Enhanced electrochemical performance of porous activated carbon by forming composite with graphene as high-performance supercapacitor electrode material. J. Nanopart. Res. **19**, 77–86 (2017)

52. Liu, D., et al.: Organic-inorganic hybrid mesoporous titanium silica material as bi-functional heterogeneous catalyst for the CO_2 cycloaddition. Fuel **244**, 196–206 (2019)

53. Dong, Z., et al.: Performance and mechanism of selective adsorption of silver to L-cysteine functionalized cellulose microsphere. Cellulose **27**, 3249–3261 (2020)

54. El-Ghaffar, M.A.A., Abdel-Wahab, Z.H., Elwakeel, K.Z.: Extraction and separation studies of silver(I) and copper(II) from their aqueous solution using chemically modified melamine resins. Hydrometallurgy **96**, 27–34 (2009)

55. Du, J.F., et al.: Facile fabrication of sodium styrene sulfonate-grafted ethylene-vinyl alcohol copolymer as adsorbent for ammonium removal from aqueous solution. Environ. Sci. Pollut. R. **25**, 27235–27244 (2018)

56. Elshehy, E.A., et al.: Selective recovery of silver(I) ions from E-waste using cubically multithiolated cage mesoporous monoliths. Eur. J. Inorg. Chem. **2017**, 4823–4833 (2017)

57. Condomitti, U., et al.: Silver recovery using electrochemically active magnetite coated carbon particles. Hydrometallurgy **147**, 241–245 (2014)

58. Abd El-Ghaffar, M.A., et al.: Adsorption of silver(I) on synthetic chelating polymer derived from 3-amino-1,2,4-triazole-5-thiol and glutaraldehyde. Chem. Eng. J. **151**, 30–38 (2009)

59. Zhang, M., et al.: Ion-imprinted chitosan gel beads for selective adsorption of Ag+ from aqueous solutions. Carbohydr. Polym. **130**, 206–212 (2015)

60. Tran, H.N., et al.: Thermodynamic parameters of cadmium adsorption onto orange peel calculated from various methods: A comparison study. J. Environ. Chem. Eng. **4**(3), 2671–3268 (2016)

61. Goldberg, S.: Inconsistency in the triple layer model description of ionic strength dependent boron adsorption. J. Colloid Interf. Sci. **285**, 509–517 (2005)

62. Al-Degs, Y.S., et al.: Effect of solution pH, ionic strength, and temperature on adsorption behavior of reactive dyes on activated carbon. Dyes Pigments **77**, 16–23 (2008)

63. An, F.Q., et al.: Selective adsorption of $AuCl_4^-$ on chemically modified D301 resin with containing N/S functional polymer. J. Environ. Chem. Eng. **5**, 10–15 (2017)

64. Villalobos, L.F., Yapici, T., Peinemann, K.V.: Poly-thiosemicarbazide membrane for gold recovery. Sep. Purif. Technol. **136**, 94–104 (2014)

65. Fu, L., et al.: Selective adsorption of Ag^+ by silica nanoparticles modified with 3-amino-5-mercapto-1,2,4-triazole from aqueous solutions. J. Mol. Liq. **241**, 292–300 (2017)

66. Rahman, M.M., et al.: Optimization, kinetic and thermodynamic studies for removal of Brilliant Red (X-3B) using tannin gel. J. Environ. Chem. Eng. **2**(1), 76–83 (2014)